A FEM Simulation Model to Calculate Local Currents and Voltages of NI REBCO Coil With Both Screening Current and Transverse Current Considered

Jeseok Bang

***Abstract*—Numerical simulations of no-insulation REBCO magnet should be able to calculate the transverse current flowing along the turn-to-turn contact path and screening current induced by the nature of superconductivity. Mataira et al. (2020) reported an invaluable finite-element model using rotated anisotropic resistivity and validated the model by comparing simulation results between the proposed model and the well-known distributed circuit network model. As a result, they addressed the key challenge of conventional analysis models, which have not calculated screening current and transverse current simultaneously. However, an insufficient part remains, as discussions of local current and voltage distributions have not yet been made. Here, we report a finite element method simulation model to address the remaining issue while numerically improving computation simplicity and speed. This model fundamentally employs H-formulation, homogenized current density domain, and homogenized contact resistivity domain, referring to the research of Mataira et al. (2020), but the definition and the supplemental conditions are incorporated to enable calculating local currents and voltages. In this article, we will validate the proposed model through numerical study and then demonstrate the model's practicability by comparing simulated and measured results.**

***Index Terms*—Coil modeling, finite element method (FEM), REBCO-coated conductor, screening current, transverse current.**

I. Introduction

NUMERICAL simulations of no-insulation (NI) $REBa_2Cu_3O_{7-x}$ (REBCO, RE=rare earth) magnets should be able to simultaneously calculate the transverse current induced by the time derivative of magnetic potential difference along the turn-to-turn contact path and screening current induced by the nature of superconductivity. In general, two simulation methods are used in the conventional numerical analysis of NI REBCO magnets, the finite element method (FEM) and the partial element equivalent circuit (PEEC) network, which are theoretically different in finding a solution. FEM simulation finds solutions of magnetic field variables by minimizing the so-called functional in an indirect way, and PEEC simulation finds solutions of current and voltages in a direct way, because of the advantages in the versatility and computation time efficiency of FEM, various models based on different electromagnetic formulations have been developed [1], [2], [3], [4], [5], [6], [7], [8], [9], [10], [11] and used to simulate screening current and its effects, e.g., screening current-induced field [12], [13], [14], [15], [16], [17], [18], [19], [20], voltage [21], and stress [22], [23], [24], [25], [26], [27]. Meanwhile, though time-consuming, PEEC is used to investigate local currents (both longitudinal and transverse) and voltages and even upon a magnet quench simulation [28], [29], [30], [31], [32], [33], [34], [35], [36], [37], [38]. One thing to note is that two methods have suffered from the issue that FEM does not consider transverse current and PEEC screening current and thus insufficient for precise analysis of NI magnets.

Numerous endeavors have been made to address the challenge. As a result, each method's limitation has been supplemented by rotated anisotropic resistivity transformation for FEM [39], [40] and by axially distributed partial elements for PEEC [41], [42], [43], [44]. However, practical issues still remain for each method. Advanced PEEC models require considerably excessive computation loads, including the calculation of mutual inductances between partial elements, leading to the severe issue that advanced PEEC simulations become too costly. For advanced FEM models, an insufficient part remains, as discussions of local current and voltage distributions have not yet been made, though validated by comparing simulation and measurement at the coil voltage level.

Here, we thus report a FEM simulation model to address the remaining issue while numerically improving computation simplicity and speed. This model fundamentally employs H-formulation, homogenized current density domain, and homogenized contact resistivity domain, referring to the research of Mataira et al. [39], but the definition and the supplemental conditions are incorporated to enable calculating local currents and voltages. In this article, we will validate the proposed model through numerical study and then demonstrate the practicability by comparing simulated and measured results.

Manuscript received 11 March 2024; revised 8 May 2024 and 29 May 2024; accepted 31 May 2024. Date of publication 4 June 2024; date of current version 17 June 2024. This work was supported in part by the National Science Foundation Cooperative performed at National High Magnetic Field Laboratory, under Agreement DMR-2128556, in part by the State of Florida, and in part by the DOE Office of Fusion Energy Sciences under Grant DE-SC0022011.

The author is with National High Magnetic Field Laboratory, Florida State University, Tallahassee, FL 32310 USA (e-mail: jbang@asc.magnet.fsu.edu).

Color versions of one or more figures in this article are available at https://doi.org/10.1109/TASC.2024.3409147.

Digital Object Identifier 10.1109/TASC.2024.3409147

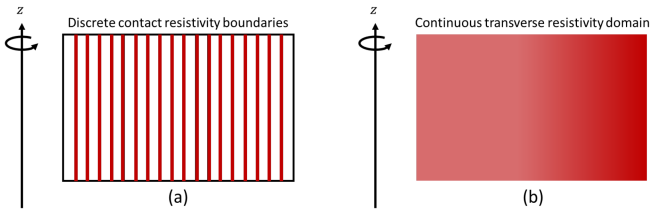

Fig. 1. Schematic drawings of a homogenized resistivity domain for a 2D-axisymmetric simulation: (a) discrete boundaries considering turn-to-turn contact surfaces and (b) equivalent homogenized and continuous domain.

II. Method

The aims of this section are twofold. We introduce a homogenized resistivity domain. This enables a FEM simulation to consider variable contact resistance that may vary by field, stress, and temperature distributions and the corresponding resistivity. Next, governing equations and boundary conditions for FEM simulation based on general partial derivative equations are summarized, required for calculating local currents and voltages of NI coils. Meanwhile, in the model validation, we assume a solenoid-shaped NI coil and a homogeneous contact resistivity on the turn-to-turn contact. In addition, it is supposed that the contact layer is the single component for contact resistance, although some layers in a REBCO-coated conductor, e.g., MgO and the electroplated layers, could be determinants of the contact resistance of an NI coil [45].

A. Homogenized Resistivity Domain

Fig. 1 presents discrete contact resistivity boundaries and continuous resistivity domain for a stack of REBCO tapes in an NI coil. Mataira et al. [39] proposed a homogenization technique dividing *constant* contact resistivity by the tape thickness for an advanced FEM simulation, which is a practical option for FEM simulation. However, we have studied that the resistivity is changed by contact pressure, temperature, and magnetic field [46], [47], [48], [49], which are inconsistent along the radial build, so this should be considered in FEM simulation. The fundamental philosophy of the homogenized resistivity domain adopted in this work is to uniformly distribute a concentrated transverse electric field at the contact surface due to contact resistivity into individual turns, thus a continuous resistivity domain. This philosophy is conceived from the domain homogenization technique proposed to mitigate computation load and time without loss of accuracy for nonuniform current density simulation [50].

The contact resistance of an NI coil is expressed as follows:

$$R_{\mathrm{c}} = \sum_{i=1}^{N} \frac{\rho_{\mathrm{ct}}[i]}{2\pi r[i] \cdot w} \tag{1}$$

where R_{c}, N, $\rho_{\mathrm{ct}}[i]$, $r[i]$, and w stand for, respectively, the contact resistance of an NI coil, the number of turns in an NI coil, contact resistivity, ith turn's radius, and REBCO tape width. The homogenized resistivity domain $\rho_r(r)$ is defined considering uniform resistivity in each turn, and the results are described as follows:

$$\frac{\rho_{\mathrm{ct}}[i]}{2\pi r[i]w} = \int_{r[i-1]}^{r[i]} \frac{\rho_r(r)}{2\pi r w} dr \tag{2}$$

$$\rho_r(r) = \frac{\rho_{\mathrm{ct}}[i]}{r[i] \ln\left(\frac{r[i]}{r[i-1]}\right)} \quad r \in \{r[i-1], r[i]\}$$

$$\approx \frac{\rho_{\mathrm{ct}}[i]}{r[i]} \cdot \frac{1}{\xi[i] - \frac{\xi[i]^2}{2} + \frac{\xi[i]^3}{3} - \frac{\xi[i]^4}{4}} \tag{3}$$

$$\xi[i] = \frac{\delta}{r[i-1]} \tag{4}$$

where δ is the REBCO tape thickness. Note that (3) is expanded considering a general case that the contact resistivity at each turn is not constant, where the last description in (3) is expressed using the Taylor series expansion considering the particular condition of $\frac{\delta}{r[i]} \ll 1$. This simple setup converts the discrete resistivity domain into the continuous domain, thus enabling the transverse electric field propagation simulation.

B. Governing Equations and Boundary Conditions

The governing equations of a 2-D axisymmetric FEM simulation for an NI REBCO solenoid coil are described with Faraday's law in a cylindrical coordinate (r, ϕ, z)

$$\begin{aligned} \mu r \frac{\partial H_r(r,z)}{\partial t} - \frac{\partial (r E_\phi(r,z))}{\partial z} &= 0 \\ \mu r \frac{\partial H_z(r,z)}{\partial t} + \frac{\partial (r E_\phi(r,z))}{\partial r} &= 0 \end{aligned} \tag{5}$$

where H_r, H_z, and E_ϕ are the basic variables of magnetic and electric fields. We assumed a negligible azimuthal magnetic field ($H_\phi \approx 0$) considering the axisymmetricity. Meanwhile, Ampère's circuital law must be satisfied in this simulation as follows:

$$J_\phi(r,z) = \frac{\partial H_r(r,z)}{\partial z} - \frac{\partial H_z(r,z)}{\partial r} \equiv \sigma_\phi(r,z) E_\phi(r,z) \tag{6}$$

where J_ϕ and σ_ϕ are the current density with screening current and the azimuthal component of resistivity in REBCO tape. Note that σ_ϕ is the nonlinear conductivity of REBCO tape varying by electric field, modeled by the power law $E - J$ relationship assuming a homogeneous medium [51]

$$E = \left(\frac{E_c}{J_c(B,\theta)}\right) \left(\frac{|J|}{J_c(B,\theta)}\right)^{n(B,\theta)-1} J \tag{7}$$

where B, θ, $J_c(B,\theta)$, and $n(B,\theta)$ are magnetic field intensity, magnetic field angle, field-dependent critical current density, and field-dependent index value for the law [52], [53], [54].

The 1-D behaviors of local currents and voltages of an NI coil in a cylindrical coordinate (r, ϕ, z) of a 2D-axisymmetric domain for a FEM simulation model are described with the following

equations:

$$V_{\phi,\text{ind}}(r) = -\frac{\partial}{\partial t}\int_{S_\phi} \mathbf{A}\cdot d\mathbf{l} = \frac{1}{\delta}\int_r^{a_1}\left\{\int_0^{2\pi}\left[\frac{1}{w}\int_w \frac{\partial A_\phi(r,z)}{\partial t}dz\right]rd\phi\right\}dr \tag{8}$$

$$V_{\phi,\text{res}}(r) = \frac{1}{\delta}\int_r^{a_1}\left\{\int_0^{2\pi}\left[\frac{1}{w}\int_w E_\phi(r,z)dz\right]rd\phi\right\}dr \tag{9}$$

$$V_{r,\text{ind}}(r) = -\frac{\partial}{\partial t}\int_{S_r}\mathbf{A}\cdot d\mathbf{l} = \int_r^{a_1}\left[\frac{1}{w}\int_w \frac{\partial A_r(r,z)}{\partial t}dz\right]dr \tag{10}$$

$$V_{\text{tot}}(r) = V_{\phi,\text{ind}}(r) + V_{\phi,\text{res}}(r) = V_{r,\text{ind}}(r) + V_r(r) \approx V_r(r) \tag{11}$$

$$E_r(r) = -\nabla V_r(r) = -\frac{\partial V_r(r)}{\partial r} \tag{12}$$

$$I_{\text{op}} = I_r(r) + I_\phi(r) = 2\pi r w\frac{1}{\rho_r(r)}E_r(r) + \left[\int_w \sigma_\phi(r,z)E_\phi(r,z)dz\right]\cdot\delta \tag{13}$$

where S_ϕ, a_1, I_{op}, I_r, and I_ϕ are the cross-sectional area, inner radius the operating, radial, and azimuthal currents of an NI coil. The inductive voltage $V_{\phi,\text{ind}}$ caused by the axial magnetic vector potential A_ϕ should be considered, but $V_{r,\text{ind}}$ is probably negligible because of the weak-coupling feature of the radial magnetic vector potential A_r. $V_{\phi,\text{ind}}$ is approximated by time-derivative and source-integral along the radial build, considering that the inductance of an NI coil can be expressed as an average of magnetic vector potential resulting from currents flowing in the coil's cross-sectional area [55]. Then, total voltage V_{tot} is described by the sum of inductive voltage V_{ind} and resistive voltage V_{res} caused by E_ϕ or E_r. Note that we assume that there is no axial gradient of E_r while nonuniform current density due to screening current is included in E_ϕ. The following equations describe magnetic vector potential $\mathbf{A}$ and magnetic field $\mathbf{B}$, which are induced by current density $\mathbf{J}$, with the given electric field variables

$$\mathbf{A} = A_r(r,z)\hat{r} + A_\phi(r,z)\hat{\phi}$$

$$\mathbf{B} = B_r(r,z)\hat{r} + B_\phi(r,z)\hat{\phi} + B_z(r,z)\hat{z} \tag{14}$$

$$\mathbf{J}(r,z) = J_r(r)\hat{r} + J_\phi(r,z)\hat{\phi} \tag{15}$$

$$A_r(r,z) = A_{r,J_r} + A_{r,J_\phi}(\equiv 0) = \int_{V'}\frac{\mu_0}{4\pi}\frac{J_r(r')\cos(\phi-\phi')}{\sqrt{r^2+r'^2-2rr'\cos(\phi-\phi')+(z-z')^2}}dv' \approx \int_{z'}\int_{r'}\frac{\mu_0 J_r(r')r'}{2}\left[\sum_{i=1}^{n_g}\omega_i f_A(\pi\xi_i+\pi)\right]dr'dz' \tag{16}$$

$$A_\phi(r,z) = A_{\phi,J_r}(\equiv 0) + A_{\phi,J_\phi} = \int_{V'}\frac{\mu_0}{4\pi}\frac{J_\phi(r',z')\cos(\phi-\phi')}{\sqrt{r^2+r'^2-2rr'\cos(\phi-\phi')+(z-z')^2}}dv' \approx \int_{z'}\int_{r'}\frac{\mu_0 J_\phi(r',z')r'}{2}\left[\sum_{i=1}^{n_g}\omega_i f_A(\pi\xi_i+\pi)\right]dr'dz' \tag{17}$$

$$B_r(r,z) = -\frac{\partial A_\phi}{\partial z} \tag{18}$$

$$B_\phi(r,z) = \frac{\partial A_r}{\partial z} = \int_{V'}\frac{\mu_0}{4\pi}\frac{J_r(r')\cos(\phi-\phi')(z-z')}{\sqrt{(r^2+r'^2-2rr'\cos(\phi-\phi')+(z-z')^2)^3}}dv' \approx \int_{z'}\int_{r'}\frac{\mu_0 J_r(r')(z-z')r'}{2}\left[\sum_{i=1}^{n_g}\omega_i f_B(\pi\xi_i+\pi)\right]dr'dz' \tag{19}$$

$$B_z(r,z) = \frac{1}{r}\frac{\partial}{\partial}(rA_\phi) \tag{20}$$

$$f_A(x) = \frac{\cos(x)}{\sqrt{r^2+r'^2-2rr'\cos(x)+(z-z')^2}} \tag{21}$$

$$f_B(x) = \frac{\cos(x)}{[r^2+r'^2-2rr'\cos(x)+(z-z')^2]^{3/2}} \tag{22}$$

where μ_0, $'$, V, ω_i, ξ_i, and n_g stand for the permeability of the vacuum, the superscription to note the given source region, volume, weights of Gauss–Legendre quadrature, points of Gauss–Legendre quadrature, and the number of points. We utilized the Gaussian–Legendre quadrature rule considering the numerical integration challenges that the angular position variable ϕ cannot be used in implementing elliptic integrals of (16)–(17) in a 2D-axisymmetric domain for FEM simulations and there is a computation singularity when the denominators become 0; this approach improves the computation speed without loss of generality and accuracy [56] if $n_g \approx 16$.

C. Simulation Setup

This work utilizes COMSOL Multiphysics to implement the proposed method. Two components, COMP1 and COMP2, are defined: one with 2D-axisymmetric space dimension and the other with 1D-axisymmetric space dimension. General form partial differential equation (PDE) and magnetic field simulation modules are added in COMP1, and a coefficient form PDE module in COMP2. COMP1 is the main component for calculating most variables, including screening current, while COMP2 supports the transverse electric field and the corresponding transverse current calculation. Nonlocal coupling definitions provided in the software, e.g., integration, linear projection, and linear extrusion, are used for numerical integral and variables' coupling, thus fully coupled calculation. In detail, linear projection and integration operators are utilized for (8)–(10) in COMP1, while linear extrusion is used to variables exchange between COMP1 and COMP2 for (12)–(13). A built-in operator

TABLE I
SIMULATION PARAMETERS FOR VALIDATION

Parmameters		
Tape width and thickness	[mm]	4;0.1
Inner and outer radii	[mm]	10;15
Number of turn and coil		50;1
Contact resistivity	[μΩcm^2]	1

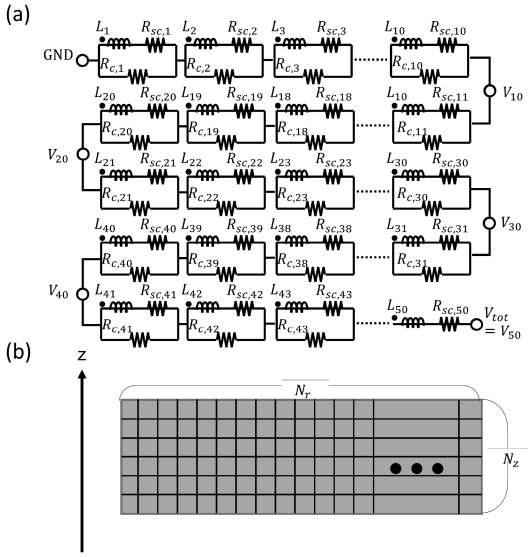

Fig. 2. Simulation setup of each method: (a) PEEC and (b) proposed FEM.

evaluating parts of an integration coupling expression on a destination side is used for the source-to-destination integral, e.g., (16) and (17). Another built-in operator is employed to ignore a symbolic differentiation engine when updating (13), a weak constraint for screening current simulation in COMP1, leading to addressing an inevitable divergence issue of a fully coupled solver. The backward differentiation formula is set to be a strict mode for an implicit solver. In addition, the Anderson mixing approach is employed for solver stabilization and acceleration.

D. Model Validation

A simple case study confirms the ability to calculate local currents and voltages of the proposed FEM model, leading to an evaluation of it as an alternative to the conventional PEEC model by comparing simulation results. For the simple comparison, we assume 1) no screening current, 2) negligible value for the power-law resistance, and 3) constant contact resistivity. Table I summarizes simulation parameters.Fig. 2 describes each simulation model. The circuit network consists of 150 components, including self-inductances, nonlinear power-law resistances, and contact resistances. In addition, $\binom{50}{2}$ mutual inductances are explicitly implemented in the stiff matrix. Accordingly, the size of the stiff matrix for the circuit simulation is basically $\binom{50}{2} \times \binom{50}{2}$. Unlike the circuit model requiring every electric component of each turn to calculate currents and voltages, however, the FEM model derives the solution with user-defined $N_r \times N_z$ finite elements probably independent of the number of turns in an NI coil.

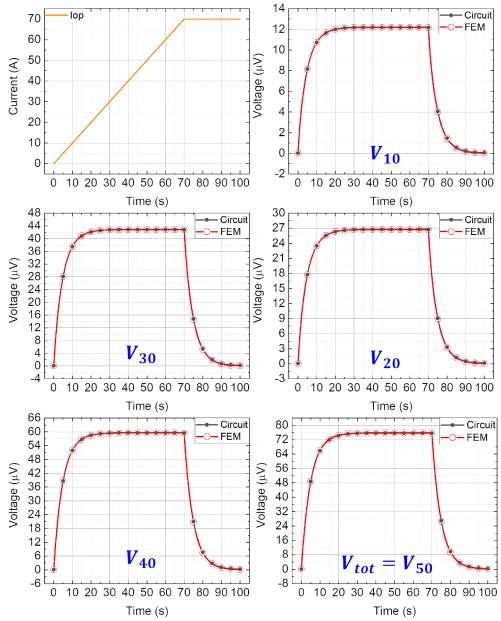

Fig. 3. Comparison between voltage simulation results by PEEC and FEM at selected locations in an NI REBCO coil.

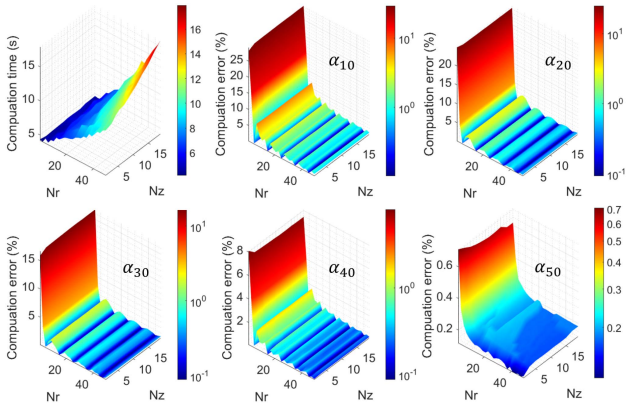

Fig. 4. Computation time and accuracy depending on N_z and N_r: computation time, α_{10}, α_{20}, α_{30}, α_{40}, and α_{50}.

Fig. 3 compares simulation results of local voltages at every ten turns in the given coil and shows a good agreement, thus validating the proposed method. It can be deduced that the simulated local currents of each model are also in good agreement based on the constant contact resistivity assumption. This work concludes that the proposed model is a competitive alternative to the circuit model. All the inductances were calculated first for the circuit simulation, while $R_{sc} \approx 0$. Second, each contact resistance at each turn was estimated by (1). Next, the solution of currents and voltages was derived. For FEM, the constant contact resistivity was transformed into a homogenized resistivity domain using (2)–(4). N_r and N_z were 50 and 16, respectively. Note that COMSOL software was adopted for both simulations while using the same solver.

Further simulations have been done to evaluate the computational performance of the proposed method compared to the conventional circuit model. Fig. 4 presents the required computation time depending on the combination of N_r and

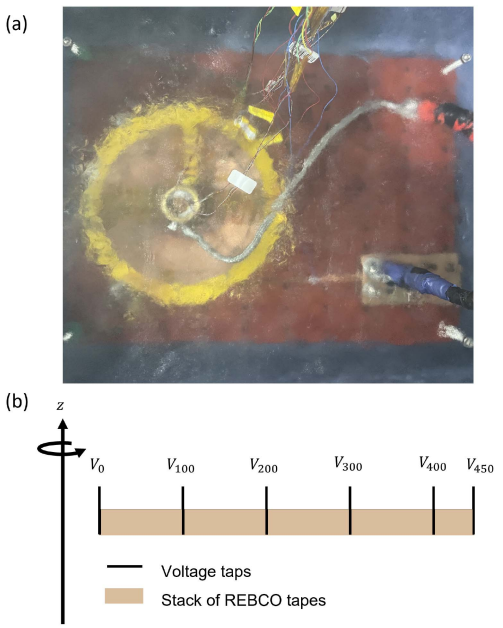

Fig. 5. (a) Coil operation in a liquid nitrogen bath and (b) schematic drawing of windings and voltage taps described in the cross-sectional view.

N_z (up to 50 and 20) and the corresponding accuracy. This evaluation defines the accuracy terminology α, assuming that the circuit simulation results are the reference, and it is set to be the maximum value of time-wise errors of voltages calculated with

$$\alpha_{i\in\{10,20,30,40,50\}} = \max\left\{\left|\frac{V_i^{\mathrm{PEEC}} - V_i^{\mathrm{FEM}}}{V_i^{\mathrm{PEEC}}}\right|\right\}_{i\in\{10,20,30,40,50\}} \tag{23}$$

where V_i^{PEEC} and V_i^{FEM} stand for voltages calculated by PEEC and FEM models at ith turn. Although there is some singularity probably caused by the so-called FEM truncation error, in general, it is confirmed the larger N_r and N_z, the less computation error and the more considerable computation time. In addition, the negligible N_z dependency on computation error is confirmed, which is supposed to be because of a uniform current density assumption. For reference, the circuit simulation time to derive the solution is about 20 s when using the same solver option with the FEM model. Another intriguing thing is the fluctuation in the computation error depending on N_r. This seems to result from the discretization setup of the shape function type and the element order. For reference, the edge element, also known as the curl element, and the quadratic order were used for the FEM simulation as a basic setup.

III. Results and Discussion

The proposed method was used to reproduce local voltages of an NI REBCO test coil, which experienced three different operation regimes, i.e., nominal, overcurrent, and sudden discharge, and thus finally validated. Fig. 5 presents a picture of the test coil, a picture of the liquid nitrogen test, and a schematic drawing of windings and voltage taps. The coil was realized with

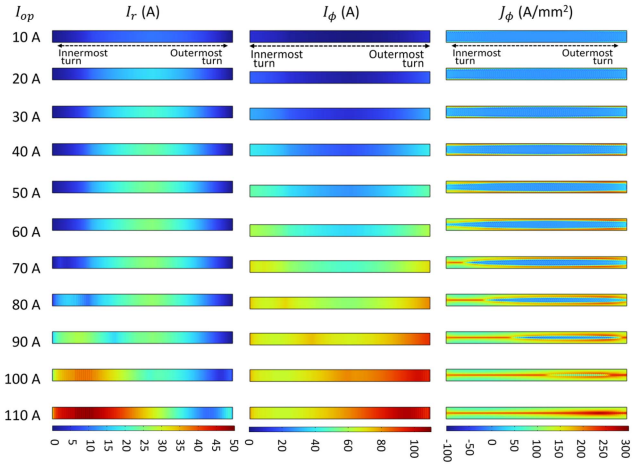

Fig. 6. Calculation results of radial current I_r, azimuthal current I_ϕ, and current density J_ϕ at selected operating currents: 10, 20, 30, 40, 50, 60, 70, 80, 90, 100, and 110 A. In the case of I_r and I_ϕ, they are expressed in 2-D expansion from 1-D.

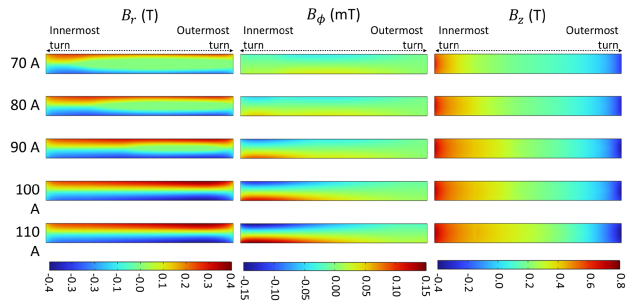

Fig. 7. Calculation results of radial magnetic field B_r, azimuthal magnetic field B_ϕ, and axial magnetic field B_z at selected operating currents in the over-current operation regime: 70, 80, 90, 100, and 110 A.

450 turns and fabricated by the NI winding technique. We used a commercial REBCO tape whose self-field critical current at 77 K is about 200 A and whose index value of the power-law resistivity is about 30 at the self-field environment. During the coil winding, voltage taps were inserted at every hundred turns, including the innermost and outermost turns. The coil operated in a liquid nitrogen bath (77 K) and charged slowly (0.05 A/s), aiming to monitor the local current sharing and its effect in the given NI test coil. The combination of over-current 110 A and sudden discharge protocols was applied, where the coil critical current was estimated as 68 A.

The FEM model was used to analyze the NI REBCO test coil while setting $N_r = 120$ and $N_z = 8$ for the simulation. Measured field-dependent critical current and local contact resistance were considered; the contact resistivity was modeled assuming a linear increase [48] considering that measured local resistances were 54.7, 21.7, 21.1, 43.0, and 71.2 $\mu\Omega$[47], sequentially. The total computation time of the FEM simulation was about 2 h. Figs. 6 and 7 presents calculation results of azimuthal current I_ϕ, radial current I_r, current density J_ϕ, and the corresponding magnetic fields described in the cross-sectional view of the test coil at selected operating currents. The local quench and its

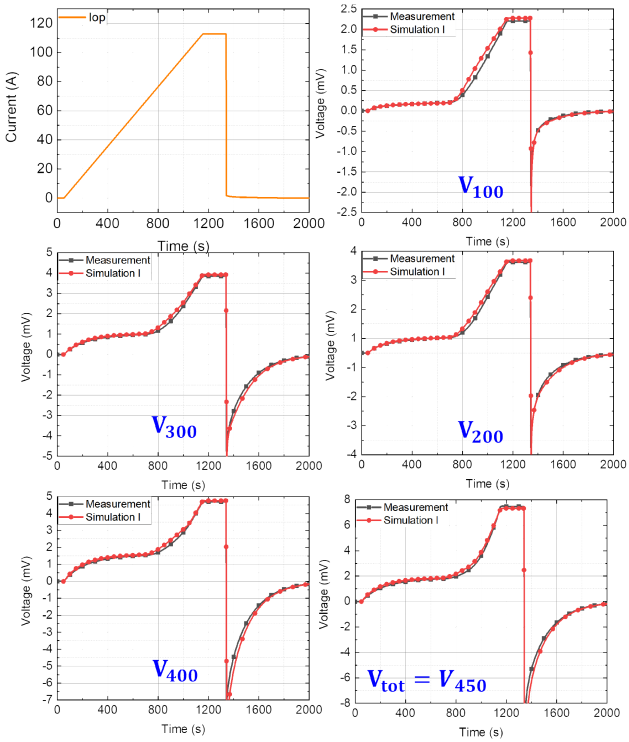

Fig. 8. Comparison between measured and simulated voltages at selected locations in an NI REBCO coil.

propagation were also simulated, where we defined that the local quench initiates if the local critical current is lower than the operating current.

Fig. 8 provides a comparison between measured and simulated results. The local voltage behavior and even the current sharing behavior in nominal, over-current, and sudden-discharge regimes were reproduced well, where the time-wise maximum error between measurement and simulation results is $<1\%$. This comparison concludes that the proposed model is practical in investigating the electromagnetic behaviors of an NI REBCO coil with screening current and transverse current considered.

Simulation results provided in Figs. 6 and 7 discuss the following.

1) The negligible variation of I_r when $I_{\text{op}} = 40$ A to 70 A is found, while notable variation by the current sharing regime when $I_{\text{op}}>70$ A.
2) The radial current during the nominal operation ($I_{\text{op}} =$ 40 A to 70 A) is mainly induced at the middle section where the magnetic potential is higher than others.
3) In the over-current regime, the radial current of the NI coil is induced comparably at the inner section where the local critical current is lower than others.
4) Screening current simulation and the corresponding voltage simulation results seem to be mainly related to the calculation results of A_ϕ, but marginally to A_r.

IV. Conclusion

The takeaways from this study are twofold. First, the FEM model incorporating screening current transverse current simulations is a promising option to reproduce local current and voltage behaviors in the general protocols of coil operation: nominal, over-current, and sudden discharge. Next, the model is simple but fast and accurate to simulate electromagnetic behaviors with field variables, while it has simulation flexibility in that users control the degree of freedom, which is related to computation time, considering a specific simulation purpose. Lastly, we can suggest that this model is applicable to the NI REBCO coil quench analysis, although it has not yet been applied to quench analysis because of the lack of data. We hope many researchers utilize this model to analyze an NI REBCO coil quench and even design an NI REBCO magnet.

References

[1] N. Amemiya, S.-i. Murasawa, N. Banno, and K. Miyamoto, "Numerical modelings of superconducting wires for AC loss calculations," *Physica C*, vol. 310, no. 1–4, pp. 16–29, 1998.
[2] R. Pecher et al., "3D-modelling of bulk type II superconductors using unconstrained H-formulation," in *Proc. 6th EUCAS Conf.*, Sorrento, Italy, Sep. 2003, pp. 1–11.
[3] D. Ruiz-Alonso, T. Coombs, and A. Campbell, "Computer modelling of high-temperature superconductors using an A–V formulation," *Supercond. Sci. Technol.*, vol. 17, no. 5, pp. S305–S310, 2004.
[4] Z. Hong, A. Campbell, and T. Coombs, "Numerical solution of critical state in superconductivity by finite element software," *Supercond. Sci. Technol.*, vol. 19, no. 12, pp. 1246–1252, 2006.
[5] R. Brambilla, F. Grilli, and L. Martini, "Development of an edge-element model for AC loss computation of high-temperature superconductors," *Supercond. Sci. Technol.*, vol. 20, no. 1, pp. 16–24, 2006.
[6] H. Zhang, M. Zhang, and W. Yuan, "An efficient 3D finite element method model based on the T–A formulation for superconducting coated conductors," *Supercond. Sci. Technol.*, vol. 30, no. 2, 2016, Art. no. 024005.
[7] F. Liang et al., "A finite element model for simulating second generation high temperature superconducting coils/stacks with large number of turns," *J. Appl. Phys.*, vol. 122, no. 4, 2017, Art. no. 043903.
[8] R. Brambilla, F. Grilli, L. Martini, M. Bocchi, and G. Angeli, "A finite-element method framework for modeling rotating machines with superconducting windings," *IEEE Trans. Appl. Supercond.*, vol. 28, no. 5, Aug. 2018, Art. no. 5207511.
[9] E. Berrospe-Juarez, V. M. Zermeño, F. Trillaud, and F. Grilli, "Real-time simulation of large-scale HTS systems: Multi-scale and homogeneous models using the T–A formulation," *Supercond. Sci. Technol.*, vol. 32, no. 6, 2019, Art. no. 065003.
[10] L. Bortot et al., "A coupled A–H formulation for magneto-thermal transients in high-temperature superconducting magnets," *IEEE Trans. Appl. Supercond.*, vol. 30, no. 5, Aug. 2020, Art. no. 4900911.
[11] D. K. Oh, "An alternative in H-formulation to the critical current model of HTS conductors," *IEEE Trans. Appl. Supercond.*, vol. 32, no. 7, Oct. 2022, Art. no. 4901808.
[12] D. Uglietti, Y. Yanagisawa, H. Maeda, and T. Kiyoshi, "Measurements of magnetic field induced by screening currents in YBCO solenoid coils," *Supercond. Sci. Technol.*, vol. 23, no. 11, 2010, Art. no. 115002.
[13] H. Ueda et al., "Spatial and temporal behavior of magnetic field distribution due to shielding current in HTS coil for cyclotron application," *IEEE Trans. Appl. Supercond.*, vol. 23, no. 3, Jun. 2013, Art. no. 4100805.
[14] G. Dilasser, P. Fazilleau, and P. Tixador, "Experimental measurement and numerical simulation of the screening current-induced field decay in a small ReBCO coil," *IEEE Trans. Appl. Supercond.*, vol. 27, no. 4, Jun. 2017, Art. no. 4900104.
[15] Y. J. Hwang et al., "A study on mitigation of screening current induced field with a 3-T 100-mm conduction-cooled metallic cladding REBCO magnet," *IEEE Trans. Appl. Supercond.*, vol. 27, no. 4, Jun. 2017, Art. no. 4701605.
[16] H. Miyazaki et al., "Screening-current-induced magnetic field of conduction-cooled HTS magnets wound with REBCO-coated conductors," *IEEE Trans. Appl. Supercond.*, vol. 27, no. 4, Jun. 2017, Art. no. 4701705.
[17] S. Kim, C. Lee, J. Bang, and S. Hahn, "Manipulation of screening currents in an (RE) $Ba_2Cu_3O_{7-x}$ superconducting magnet," *Mat. Res. Exp.*, vol. 6, no. 2, 2018, Art. no. 026004.

[18] J. Bang et al., "Field measurement and analysis of a 3 T 66 mm no-insulation HTS NMR magnet with screening current and manufacturing uncertainty considered," *IEEE Trans. Appl. Supercond.*, vol. 29, no. 5, Aug. 2019, Art. no. 4601305.
[19] J. Bang et al., "A numerical method to calculate spatial harmonic coefficients of magnetic fields generated by screening currents in an HTS magnet," *IEEE Trans. Appl. Supercond.*, vol. 30, no. 4, Jun. 2020, Art. no. 4901405.
[20] J. Y. Jang et al., "Reproducibility of the field homogeneity of a metal-clad no-insulation all-REBCO magnet with a multi-layer ferromagnetic shim," *Supercond. Sci. Technol.*, vol. 33, no. 2, 2020, Art. no. 025005.
[21] J. Bang, J. Park, K. Choi, G. Kim, and S. Hahn, "A numerical method to calculate screening current-dependent self and mutual inductances of REBCO coils," *Supercond. Sci. Technol.*, vol. 36, no. 8, 2023, Art. no. 085003.
[22] S. Hahn et al., "45.5-tesla direct-current magnetic field generated with a high-temperature superconducting magnet," *Nature*, vol. 570, no. 7762, pp. 496–499, 2019.
[23] X. Hu et al., "Analyses of the plastic deformation of coated conductors deconstructed from ultra-high field test coils," *Supercond. Sci. Technol.*, vol. 33, no. 9, 2020, Art. no. 095012.
[24] S. Takahashi et al., "Hoop stress modification, stress hysteresis and degradation of a REBCO coil due to the screening current under external magnetic field cycling," *IEEE Trans. Appl. Supercond.*, vol. 30, no. 4, Jun. 2020, Art. no. 4602607.
[25] Y. Yan et al., "Screening current effect on the stress and strain distribution in REBCO high-field magnets: Experimental verification and numerical analysis," *Supercond. Sci. Technol.*, vol. 33, no. 5, 2020, Art. no. 05LT02.
[26] J. Park, J. Bang, U. Bong, J. Kim, D. Abraimov, and S. Hahn, "Parametric study on effect of friction and overbanding in screening current stress of LBC magnet," *IEEE Trans. Appl. Supercond.*, vol. 31, no. 5, Aug. 2021, Art. no. 4603205.
[27] D. Kolb-Bond et al., "Screening current rotation effects: SCIF and strain in REBCO magnets," *Supercond. Sci. Technol.*, vol. 34, no. 9, 2021, Art. no. 095004.
[28] T. Wang et al., "Analyses of transient behaviors of no-insulation REBCO pancake coils during sudden discharging and overcurrent," *IEEE Trans. Appl. Supercond.*, vol. 25, no. 3, Jun. 2015, Art. no. 4603409.
[29] Y. Wang, H. Song, D. Xu, Z. Li, Z. Jin, and Z. Hong, "An equivalent circuit grid model for no-insulation HTS pancake coils," *Supercond. Sci. Technol.*, vol. 28, no. 4, 2015, Art. no. 045017.
[30] S. Noguchi et al., "Experiment and simulation of impregnated no-insulation REBCO pancake coil," *IEEE Trans. Appl. Supercond.*, vol. 26, no. 4, Jun. 2016, Art. no. 4601305.
[31] T. Oki et al., "Evaluation on quench protection for no-insulation REBCO pancake coil," *IEEE Trans. Appl. Supercond.*, vol. 26, no. 4, Jun. 2016, Art. no. 4702905.
[32] M. Cho et al., "Combined circuit model to simulate post-quench behaviors of no-insulation HTS coil," *IEEE Trans. Appl. Supercond.*, vol. 29, no. 5, Aug. 2019, Art. no. 4901605.
[33] S. Noguchi, "Electromagnetic, thermal, and mechanical quench simulation of NI REBCO pancake coils for high magnetic field generation," *IEEE Trans. Appl. Supercond.*, vol. 29, no. 5, Aug. 2019, Art. no. 4602607.
[34] C. Im et al., "An inverse calculation study on post-quench behavior of a no-insulation REBCO insert," *IEEE Trans. Appl. Supercond.*, vol. 30, no. 4, Jun. 2020, Art. no. 4703205.
[35] D. Liu, D. Li, W. Zhang, H. Yong, and Y. Zhou, "Electromagnetic-thermal-mechanical behaviors of a no-insulation double-pancake coil induced by a quench in the self field and the high field," *Supercond. Sci. Technol.*, vol. 34, no. 2, 2021, Art. no. 025014.
[36] S. An et al., "Fast distributed simulation of 'defect-irrelevant' behaviors of no-insulation HTS coil," *IEEE Trans. Appl. Supercond.*, vol. 31, no. 5, Aug. 2021, Art. no. 4601605.
[37] G. Kim et al., "A numerical method for spatially-distributed transient simulation to replicate nonlinear 'defect-irrelevant' behaviors of no-insulation HTS coil," *Supercond. Sci. Technol.*, vol. 34, no. 11, 2021, Art. no. 115004.
[38] G. Kim et al., "Fast current distribution simulation method for no-insulation HTS coil with defects," *IEEE Trans. Appl. Supercond.*, vol. 32, no. 6, Sep. 2022, Art. no. 4602905.
[39] R. Mataira, M. Ainslie, R. Badcock, and C. Bumby, "Finite-element modelling of no-insulation HTS coils using rotated anisotropic resistivity," *Supercond. Sci. Technol.*, vol. 33, no. 8, 2020, Art. no. 08LT01.
[40] S. Venuturumilli, R. Mataira, R. Taylor, J. Gonzales, and C. Bumby, "Modeling HTS non-insulated coils: A comparison between finite-element and distributed network models," *AIP Adv.*, vol. 13, no. 3, 2023, Art. no. 035317.
[41] S. Otten and F. Grilli, "Simple and fast method for computing induced currents in superconductors using freely available solvers for ordinary differential equations," *IEEE Trans. Appl. Supercond.*, vol. 29, no. 8, Dec. 2019, Art. no. 8202008.
[42] S. Noguchi, H. Ueda, S. Hahn, A. Ishiyama, and Y. Iwasa, "A simple screening current-induced magnetic field estimation method for REBCO pancake coils," *Supercond. Sci. Technol.*, vol. 32, no. 4, 2019, Art. no. 045007.
[43] L. Qin et al., "Refined circuit model for current distribution of the no-insulation HTS insert magnet," *Supercond. Sci. Technol.*, vol. 34, no. 7, 2021, Art. no. 075002.
[44] S. Noguchi and S. Hahn, "A newly developed screening current simulation method for REBCO pancake coils based on extension of PEEC model," *Supercond. Sci. Technol.*, vol. 35, no. 4, 2022, Art. no. 044005.
[45] A. Musso, J. Bang, N. Riva, Y. Yan, J. T. Lee, and S. Hahn, "The roles of contact resistivity and tape architecture on transverse resistance of an NI HTS coil," *IEEE Trans. Appl. Supercond.*, vol. 34, no. 5, Aug. 2024, Art. no. 4600705.
[46] J. Bang et al., "A customized electric heater to mitigate screening current by optimal control on temperature distribution in a high-temperature superconductor coil," *J. Appl. Phys.*, vol. 132, no. 18, 2022, Art. no. 183911.
[47] J. Bang et al., "A real-time monitoring system for investigating electromagnetic behaviors of an HTS coil," *IEEE Trans. Appl. Supercond.*, vol. 32, no. 6, Sep. 2022, Art. no. 9001505.
[48] J. Bang et al., "Experiment and analysis on temperature-dependent electric contact resistivity of an NI HTS coil," *IEEE Trans. Appl. Supercond.*, vol. 33, no. 5, Aug. 2023, Art. no. 6602105.
[49] J. Bang, G. Bradford, J. Lee, and D. Abraimov, "An experimental study to investigate magnetic field and winding force-dependent contact resistance of NI REBCO coil," *Supercond. Sci. Technol.*, vol. 37, no. 2, 2024, Art. no. 025008.
[50] V. M. Zermeno, A. B. Abrahamsen, N. Mijatovic, B. B. Jensen, and M. P. Sørensen, "Calculation of alternating current losses in stacks and coils made of second generation high temperature superconducting tapes for large scale applications," *J. Appl. Phys.*, vol. 114, no. 17, 2013, Art. no. 173901.
[51] J. Rhyner, "Magnetic properties and AC-losses of superconductors with power law current–voltage characteristics," *Physica C*, vol. 212, no. 3-4, pp. 292–300, 1993.
[52] F. Liang et al., "Vortex shaking study of REBCO tape with consideration of anisotropic characteristics," *Supercond. Sci. Technol.*, vol. 30, no. 9, 2017, Art. no. 094006.
[53] Y. Liu et al., "Comparison of 2D simulation models to estimate the critical current of a coated superconducting coil," *Supercond. Sci. Technol.*, vol. 32, no. 1, 2018, Art. no. 014001.
[54] J. Bang et al., "The effect of field-dependent n-value on screening current, voltage, and magnetic field of REBCO coil," *IEEE Trans. Appl. Supercond.*, vol. 34, no. 5, Aug. 2024, Art. no. 4902105.
[55] C. Hoer and Y. Love, "Exact inductance equations for rectangular conductors with applications to more complicated geometries," *J. Res. Natl Bur. Stand. C*, vol. 69, no. 2, pp. 127–137, 1965.
[56] M. W. Garrett, "Calculation of fields, forces, and mutual inductances of current systems by elliptic integrals," *J. Appl. Phys.*, vol. 34, no. 9, pp. 2567–2573, 1963.